

Steady-State Characteristics of Gas-Lubricated, Self-Acting, Partial-Arc Journal Bearings of Finite Width

By V. CASTELLI,¹ C. H. STEVENSON,² and E. J. GUNTER, JR.³

This paper contains the description of a solution of the problem of self-acting, gas-lubricated, partial-arc, finite length journal bearings for steady-state conditions.

The results can be used for bearings of many types such as simple, fixed, partial-arc journal bearings (tapered land), axial-grooved journal bearings, pivoted-pad journal bearings, and similar geometric shapes.

Sample results are plotted, and their utilization for various bearing types is illustrated by examples.

Nomenclature

A	coefficient
a_e	iteration increment
B	coefficient
b_e	total growth indicator
C^*	coefficient
C_L	load coefficient = $W/(P_a RL)$
C_{LT}	total load coefficient
C	ground clearance = $R_{\text{shoe}} - R_{\text{shaft}}$
C'	pivot circle clearance = $R_{\text{pivot}} - R_{\text{shaft}}$
D	coefficient
E_{ij}	Reynolds difference equation coefficient
e	shaft eccentricity with respect to shoe circle
e'	shaft eccentricity with respect to pivot circle
F_{ij}	Reynolds difference equation coefficient
F_o	frictional force
H	dimensionless local film thickness = h/C
H_P	dimensionless pivot film thickness h_P/C
H_T	dimensionless trailing edge film thickness = h_T/C
i	grid point in θ direction
j	grid point in axial direction
k	iteration number
L	bearing axial width
l, l	iteration number
M	number of grid cells in θ direction
N	number of grid cells in axial direction
P	dimensionless pressure = p/P_a

P_a	ambient pressure
R	shaft radius
S	coefficient
T	coefficient
W	total load
W_c	load component parallel to line of centers
W_s	load component normal to line of centers
Y	axial coordinate
α	shoe angular extent
β	angle between pivot and vertical axis
γ	relaxation factor
δ	attitude angle
ϵ	eccentricity ratio = e/C
ϵ'	eccentricity ratio = e'/C'
η	dimensionless axial coordinate = y/L
θ	angular coordinate
Λ	bearing number = $(6 \mu \omega R^2)/(P_a C^2)$
Λ_T	bearing number based on h_T , $\Lambda_T = \Lambda/H_T^2$
μ	absolute viscosity of lubricant
ξ	lead angle between line of centers and shoe leading edge
ξ_0	same as above for first pad of grooved bearing
ξ_0'	angle between load line and leading edge of first pad of grooved bearing
ϕ	angle between shoe leading edge and pivot point
ω	shaft angular velocity

Introduction

THE increasing demands of space-age technology have fostered impressive developments in the field of compressible fluid-film lubrication. It is now recognized that many properties of gas-lubricated bearings make them attractive for certain particular applications. Most of the very simple bearing geometries have been investigated to the extent that reliable design information exists, both of analytical and experimental nature. However, it is also true that gas-lubricated bearings require accurate alignment of the shaft and bearing assembly and that many of them are prone to develop a self-excited film instability.

Presented as an American Society of Lubrication Engineers paper at the Lubrication Conference held in Rochester, New York, October 15-17, 1963.

¹ Principal Engineer, The Franklin Institute, Phila. 3, Penna. and Asst. Professor, Dept. of Mechanical Engineering, Columbia University, New York.

² Bearing Analyst, Mechanical Technology, Inc., Latham, New York.

³ Research Engineer, The Franklin Institute, Philadelphia 3, Penna.

The alignment requirement has more implications than simply the need for initial parallelism of shaft and bearings. Subsequent distortion of the bearing housing and supporting structures due to transient stresses and thermal gradients may produce this critical condition. Maintaining a high degree of alignment with some bearing-structure designs is very difficult and may in some extreme cases be impossible.

The question of film instability can also be very serious. It has frequently been the major obstacle to successful bearing performance. The instability phenomenon, especially of the so-called half-frequency variety, is most pronounced in the simplest geometries such as the 360° journal bearing.

Information now available, based on limited theoretical knowledge and scattered experimental data, indicates that deviations from the basic plain cylindrical geometry improve the bearing whirl stability characteristics.

This report is concerned with the determination of basic characteristics of partial-arc, cylindrical bearings which are somewhat resistant to the difficulties described above. This in turn leads to the design of bearings with three important geometries: tilting pad, axial grooved, and fixed partial-arc (tapered land) journal bearings. All of these geometries present favorable features with respect to the stability problem, and the pivoted-pad bearing, in addition, can operate with considerable misalignment. Theoretical solutions of the complete steady-state characteristics of gas-lubricated, partial-arc bearings are not presently available, and it is felt that this will make a contribution to the advancement of the state of the art.

The film pressure generated by a self-acting, gas-lubricated bearing is governed by the well-known isothermal Reynolds lubrication equation. For compressible lubricants this equation is a nonlinear, nonhomogeneous, partial differential equation with variable coefficients, for which analytical solutions are available only in a few limiting cases.

Many approximate methods are available for the solution of Reynolds' equation. One group of these methods takes advantage of the smallness of some bearing parameter. For example, a "small ϵ expansion" has been successfully attempted by the authors and furnishes data for the region $\epsilon < 0.4$. (Note: the symbol ϵ is the eccentricity ratio of the journal in its bearing.)

Other methods of solution, such as those utilizing truncated series expansions and integral fits such as Galerkin's technique, would be very useful in obtaining close approximations to the load-carrying capacity of a bearing with any geometry. However, the basic drawback of these approximate methods is that, although the overall pressure load can be predicted quite accurately, the actual shape of the pressure profile, and consequently the position of the point of application of the load, is difficult to obtain. This argument must be considered quite seriously in cases where the static data have to be used in dynamical analysis. Then derivatives of the pressure

profiles are necessary, and the accuracy of the calculations depends considerably on the smoothness of the data and on the close similarity of the approximate and exact pressure profiles.

On the basis of these considerations the direct numerical method of solution of the exact equation governing the problem was chosen as the one best satisfying all of the accuracy requirements.

In the reported analysis, the Reynolds differential equation is reduced to a finite difference equation by standard methods. The work follows the same approach as Gross (2). Plots of the results are presented in a form convenient for use in design.

Analysis

THE REYNOLDS EQUATION

The basic theory utilizes the well-discussed assumptions concerning neglect of the inertia forces and temperature variations throughout the film. Then, the Reynolds equation can be represented in the following dimensionless form:

$$\frac{\partial}{\partial \theta} \left(PH^3 \frac{\partial P}{\partial \theta} \right) + \frac{R^2}{L^2} \frac{\partial}{\partial \eta} \left(PH^3 \frac{\partial P}{\partial \eta} \right) = \Lambda \frac{\partial PH}{\partial \theta} \quad [1]$$

with the boundary conditions (see Fig. 1):

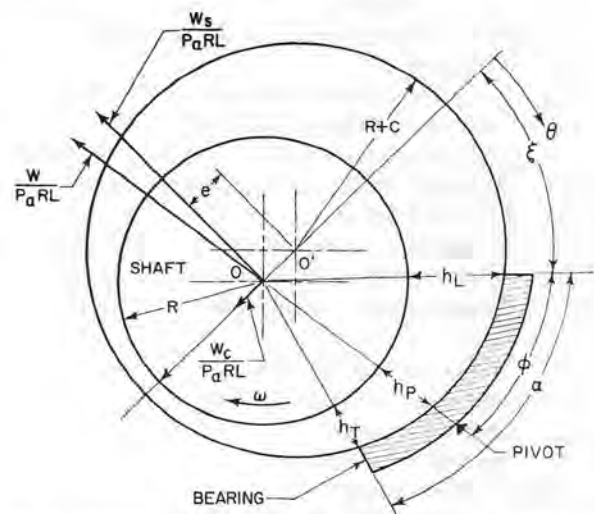


FIG. 1. Schematic diagram of a pivoted-pad bearing configuration.

$$\begin{aligned} P(\theta = \xi, \eta) &= 1 \\ P(\theta = \xi + \alpha, \eta) &= 1 \\ P(\theta = \theta, \eta = \pm 1/2) &= 1 \end{aligned} \quad [2]$$

Equation [1] can be reduced, by finite difference techniques, to the difference equation:

$$P_{i,j}^2 - 2E_{i,j}P_{i,j} + F_{i,j} = 0 \quad [3]$$

Solving Eq. [3] for $P_{i,j}$, the pressure at any point yields:

$$P_{i,j} = E_{i,j} + (E_{i,j}^2 - F_{i,j})^{1/2} \quad [4]$$

where the coefficients $E_{i,j}$ and $F_{i,j}$ can be expressed as:

$$E_{i,j} = \frac{1}{2D(\Delta\theta)^2} [P_{i+1,j} + P_{i-1,j}] + \frac{3}{4D(\Delta\theta)H_i} \left(\frac{dH}{d\theta} \right)_i [P_{i+1,j} - P_{i-1,j}] + \frac{1}{2D(\Delta\eta)^2} \left(\frac{R}{L} \right)^2 [P_{i,j+1} - P_{i,j-1}] - \frac{\Lambda}{2D} \frac{1}{H_i^3} \left(\frac{dH}{d\theta} \right)_i \quad [5]$$

$$F_{i,j} = \frac{\Lambda}{2D(\Delta\theta)H_i^2} (P_{i+1,j} - P_{i-1,j}) - \frac{1}{4D(\Delta\theta)^2} (P_{i+1,j} - P_{i-1,j})^2 - \frac{1}{4D(\Delta\eta)^2} \left(\frac{R}{L} \right)^2 [P_{i,j+1} - P_{i,j-1}]^2 \quad [6]$$

$$\text{where } D = 2 \left[\frac{1}{(\Delta\theta)^2} + \left(\frac{R}{L} \right)^2 \frac{1}{(\Delta\eta)^2} \right] \quad [7]$$

Equation [4] applied to all points of the bearing grid yields a set of simultaneous equations which can be solved by an iterative process.

At this point it is important to make a basic decision between two methods of attack:

(a) Fix the geometrical characteristics of the bearing film and the relative speed and let the pressure distribution and center of pressure be a consequence.

(b) Fix the geometrical characteristics of the shaft and bearing and the position of the center of pressure and let the bearing be free to assume any tilt as to comply with the specified data.

Method (a) was chosen because it is much simpler to program, converges more easily, does not get involved with double-valued problems, and usually gives an answer in half the time employed by method (b). The adopted method has the disadvantage of not producing direct data for a specified center of pressure position as would be desirable for the solution of a single pivoted-pad bearing problem. However, since the production of extensive field maps was the aim of the project, the data necessary for the study of pivoted-pad bearings can be easily obtained by cross-plotting.

If the production of a limited set of data for a particular pivot pad geometry is desired, it is more convenient to program the problem according to method (b).

CONVERGENCE

As is common with iterative processes, the determination and careful control of the rate of convergence is vital to successful production runs. Moreover, if the produced data must be employed in extensive cross-plotting,

smoothness and accuracy are essential. The criterion for truncation must be so selected as to stop all iteration processes at a uniform "distance" from the exact answer. Since the exact answer is not known, fictitious criteria must be selected which, nonetheless, are required to be equally effective.

The following presentation expounds one such criterion based on the exponential nature of the solutions generated by this iterative technique. The convergence of the selected iterative process is determined in the following manner:

Let the "iteration increment" at step k be defined as

$$a_i = \frac{\sum_{i,j} |P_{i,j}^{(k)} - P_{i,j}^{(k-1)}|}{\sum_{i,j} P_{i,j}^0} \quad [8]$$

where the superscript "0" refers to the initial pressure distribution.

This is, in essence, the average growth of the pressure at a non-boundary point within the bearing. Let the "total growth indicator" at step k be defined as

$$b_k = \sum_{l=1}^k a_l \quad [9]$$

This indicator measures the average total growth of the pressure profile after k iterations.

The successive iterations of the solution of Reynolds' equation as produced by either the "simultaneous displacement" or "over-relaxation" techniques have been found to behave locally exponentially with respect to the step number k . This fact can be used for the individual extrapolation of local pressure values toward the asymptotic solution in a manner akin to the "Atkin process" (3). Moreover, it can be speculated that, if the individual pressure points behave exponentially, also the total growth indicator might show the same effect. Then the following formula can be fitted to the data:

$$b_i + Ae^{-B} = b_\infty \quad [10]$$

Applying Eq. [10] to three sequential steps and eliminating the constants, one can obtain the following relation:

$$\frac{\ln [(b_1 - b_2)/(b_\infty - b_1) + 1]}{\ln [(b_1 - b_3)/(b_\infty - b_1) + 1]} = \frac{l_2 - l_1}{l_3 - l_1} \quad [11]$$

For the particular case where the steps are successive or equally spaced

$$l_2 - l_1 = l_3 - l_2 \quad [12]$$

Solving for b_∞ from Eq. [11] results in

$$b_\infty = \frac{(b_2)^2 - b_1 b_3}{2b_2 - (b_1 + b_3)} \quad [13]$$

Using this approach, the convergence is defined as

$$\frac{b_{\infty} - b_i}{b_i} < \delta \quad [14]$$

where δ is a number produced by a predetermined convergence criterion.

The advantage afforded by this technique consists of the fact that $b_{\infty} - b_i$ is a measure of how "far" the iteration solution is from the exact one. Of course, it could be observed that the solution does not exactly behave according to the above-mentioned, exponential law and that b_{∞} is indeed $b_{\infty} = b_{\infty}(k)$, $k =$ iteration number. However, but for the first few steps, b_{∞} is a very weak function of the step number and converges to the asymptote from above as opposed to $b\bar{b}$ which converges to the asymptote from below.

NUMERICAL STABILITY AND PRESSURE EXTRAPOLATION

The selection of an iteration method was made along the following lines:

(a) Simultaneous displacement techniques were chosen over successive displacement ones due to poor properties presented by the latter in connection with the numerical stability program.

(b) A process which could be suitable for both over-relaxation and under-relaxation had to be selected due to the uncertain numerical stability behavior of the solution.

Processes such as "simultaneous relaxation implicit by lines" and the "alternating gradient" method (same as the relaxation implicit by lines but in alternating directions) (3), were tried but produced mixed results and were discarded.

The growth of the pressure at a particular grid point is controlled by the following equation:

$$\bar{P}_{i,j}^{(m+1)} = \gamma P_{i,j}^{(m+1)} + (1 - \gamma) P_{i,j}^m \quad [15]$$

where $\bar{P}_{i,j}^{(m+1)}$ is the assigned value of the pressure at the point i,j for the $(m + 1)$ th iteration. $P_{i,j}^{(m+1)}$ is the calculated value of the pressure at the point i,j for the $(m + 1)$ th iteration, $P_{i,j}^m$ is the value of the pressure at the point i,j for the (m) th iteration.

From Eq. [15], it can be seen that for $\gamma = 1$, the assigned value of the pressure at the point i,j is identical to the calculated value.

Numerical instability in the iterative process is detected by an increase of the value of the iteration increment aa_k (as defined in Eq. [8]). This term normally behaves as an exponential and only when numerical instability is present does it increase rather than decrease. Usually, instability can be eliminated by lowering sufficiently the value of γ . This attenuates the effects of erratic higher harmonics of the solution and induces stability. As a result of lowering the value of γ , the iteration proceeds at a slower but more stable rate. The speed of convergence is greatest when the highest value of γ for stable iteration is used. This statement holds true in relaxation processes

for most elliptic equations departing from the simple Laplace equation and for which the process "optimum over-relaxation" does not apply.

With all of the previously mentioned conditions imposed, the number of iterations required for the solution of the system of Reynolds' difference equations varies depending upon the bearing parameters, the number of grid points, and the numerical stability of the iterative process. In order to reduce the number of required iterations, the exponential behavior of the solution was exploited. The use of the exponential extrapolation is successful in most cases but always had to be applied on a trial basis due to the occasional accentuation of local irregularities into large errors. Local exponential extrapolation was accomplished by the following equation:

$$P_{i,j}^{(n)} + Ae^{(-Bt_n)} = P_{i,j}^{(\infty)} \quad [16]$$

where

$P_{i,j}^{(n)}$ is the pressure of the point, i,j , at the n th iteration

$P_{i,j}^{(\infty)}$ is the exponential asymptote of the pressure of the point i,j

t_n is the time at the n th iteration.

Use of the same technique that was applied to Eq. [10] results in the following expression:

$$P_{i,j}^{(\infty)} = \frac{(P_{i,j}^{(2)}) - P_{i,j}^{(1)} P_{i,j}^{(3)}}{2P_{i,j}^{(2)} - (P_{i,j}^{(1)} + P_{i,j}^{(3)})} \quad [17]$$

The superscripts (1), (2), and (3) denote three equally spaced iterations in this sequence at any point in the iterative process and not necessarily the first, second and third ones. Usually $P_{i,j}$ is only an approximation to the exact solution of the governing difference equation and more relaxation steps have to be applied in order to satisfy the desired truncation criterion.

Judicious application of the extrapolation routine has been found to be the most useful single expedient in the solution of this class of problems. Extreme care must be exercised in extrapolating only grids which are proceeding very smoothly and which do not present any irregularities or "seeds of instability". In view of what has been said above, it can be concluded that the most convenient technique to follow is to adjust grid size and relaxation factor (γ) so as to start the solution on a very stable basis (values of γ corresponding to very underrelaxed conditions). A few iterations will then set the basis for extremely successful extrapolations. The stable relaxation process can be applied again, followed after a few steps by another extrapolation, and so forth. The establishment of a proper sequence is rather empirical but important for economization of valuable machine time in large production runs.

It is important to note that experience with extrapolation was less successful with geometries which involved convergent-divergent films than with the simply convergent or simply divergent ones. An example of the use of pressure extrapolation can be seen in Fig. 2. At

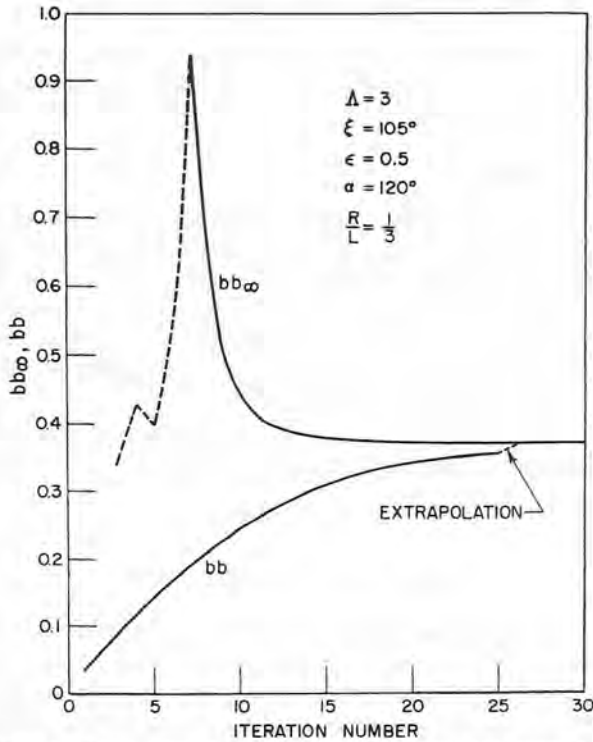


FIG. 2. Total growth indicator and extrapolated growth indicator vs. iteration number.

the 25th iteration, the extrapolation routine was applied and the step in the total growth indicator curve is indicative of the reduction of the number of required iterations.

STEADY-STATE BEARING CHARACTERISTICS

Once satisfactory convergence of the pressure profile over the bearing surface is obtained, it is possible to solve for the bearing characteristics. The load capacity for the bearing is defined as

$$\frac{W}{p_a RL} = \left[\left(\frac{W_C}{p_a RL} \right)^2 + \left(\frac{W_S}{p_a RL} \right)^2 \right]^{1/2} \quad [18]$$

where

$$\frac{W_C}{p_a RL} = \int_{-1/2}^{1/2} \int_{\xi}^{\xi+\alpha} (P-1) \cos \theta \, d\theta \, d\eta \quad [19]$$

$$\frac{W_S}{p_a RL} = \int_{-1/2}^{1/2} \int_{\xi}^{\xi+\alpha} (P-1) \sin \theta \, d\theta \, d\eta \quad [20]$$

The frictional coefficient is defined as

$$c_f = \frac{F_c}{\mu R^2 \omega L} = \int_{-1/2}^{1/2} \int_{\xi}^{\xi+\alpha} \left[H^{-1} - \frac{3}{\Lambda} (P-1) \frac{dH}{d\theta} \right] d\theta \, d\eta \quad [21]$$

These integrations are performed by Simpson's rule.

Moreover, the knowledge of the load components can be utilized to establish the position of the center of pressure with respect to the bearing.

General considerations for application of computer data

The characteristics of gas-lubricated, self-acting, cylindrical, partial-arc journal bearings have wherever possible been identified by standard terminology. However, there are certain parameters used in this report that are unique to these bearings. These parameters are defined in the text that follows:

THE PIVOT CIRCLE CLEARANCE, C'

This parameter establishes the relative position of the pivotal point (taken on the bearing surface) of tilting pad shoes with respect to the shaft. The definition of C' is

$$C' = R_{\text{pivot}} - R_{\text{shaft}} \quad [22]$$

where R_{pivot} is the distance from the pivotal point to a properly selected point fixed with respect to the bearing mounts. For the case of three shoe arrangements R_{pivot} is the radius of the circle passing through the three pivot points. R_{shaft} is the shaft radius.

THE GROUND CLEARANCE C

This is defined as the difference in radii of the bearing and shaft surfaces: $C = R_{\text{bearing}} - R_{\text{shaft}}$.

THE DIMENSIONLESS PIVOTAL FILM THICKNESS H_p

The film thickness at the center of pressure or pivot position is an important parameter in determining the operation of the bearing. For a fixed shaft position it will remain a constant regardless of the attitude of the bearing pad with respect to the pivotal circle. In agreement with the geometry of Fig. 1 this film thickness can be written as:

$$H_p = [c + e \cos(\xi + \phi)]/c \quad [23]$$

THE PAD POSITION ANGLE ξ

ξ is defined as the angle drawn from the line of centers of the bearing and shaft circles to the leading edge of the pad.

TRAILING EDGE BEARING NUMBER Λ_T

The parameter "trailing edge bearing number" is defined algebraically as

$$\Lambda_T = \frac{6 \mu \omega}{p_a} (R/h_T)^2 \quad [24]$$

where

$$h_T = C[1 + \epsilon \cos(\xi + \alpha)] \quad [25]$$

therefore,

$$\Lambda_T = \Lambda/H_T^2 \quad [26]$$

This number more closely represents the operation of an individual shoe from the conventional compressibility bearing number point of view.

THE CLEARANCE RATIO C'/C

This parameter is defined as the ratio of the pivotal circle clearance to the ground clearance. It is important because it measures the amount of preload existing due to the initial pivot circle adjustment. As an example, consider a three shoe bearing system in which each shoe has an angular extent of 120° . The film thickness at the pivots can be expressed as

$$h_{P_1}' = C'[1 + \epsilon' \cos \chi] = h_{P_1} = CH_{P_1} \quad [27]$$

$$h_{P_2}' = C'[1 + \epsilon' \cos (\chi + 120^\circ)] = h_{P_2} = CH_{P_2} \quad [28]$$

$$h_{P_3}' = C'[1 + \epsilon' \cos (\chi + 240^\circ)] = h_{P_3} = CH_{P_3} \quad [29]$$

Summing Eqs. [27], [28], and [29] yields the following:

$$H_{P_1} + H_{P_2} + H_{P_3} = (C/C') \{3 + \epsilon' [\cos \chi + \cos (\chi + 120^\circ) + \cos (\chi + 240^\circ)]\} \quad [30]$$

Performing the trigonometric substitutions yields

$$\frac{C'}{C} = \frac{H_{P_1} + H_{P_2} + H_{P_3}}{3} \quad [31]$$

This formula cannot be used if the spacing between pivots is not equal. Indeed, for the more general case in which symmetry exists about a vertical plane only, formula [31] becomes

$$\frac{C'}{C} = \frac{H_{P_1} + H_{P_2} + (2 \cos \beta) H_{P_3}}{2(1 + \cos \beta)} \quad [32]$$

where 2β is the angle between pivots 1 and 2.

PIVOTAL CIRCLE ECCENTRICITY RATIO ϵ'

The pivotal circle eccentricity ratio is defined as the relative location of the shaft center with reference to the pivotal circle center.

Design data

The data obtained from this analysis can be presented in many different arrangements. Three basic types of plots are presented in this report. They consist of plots of (a) load coefficient (C_L) vs. center of pressure position (ϕ/α); (b) pivotal film thickness (H_P) vs. center of pressure position (ϕ/α); (c) trailing film thickness (H_T) vs. center of pressure position (ϕ/α).

All plots of the (a), (b), and (c) variety contain lines of constant ϵ and lines of constant ξ . Since

$$C_L = f(\epsilon, \xi, \Lambda, R/L, \alpha)$$

and

$$\phi/\alpha = g(\epsilon, \xi, \Lambda, R/L, \alpha)$$

etc., the best a two-dimensional plot can do is to present C_L vs. ϕ/α on lines of constant ϵ and lines of constant ξ while Λ , R/L , and α must have assigned values on each graph. It should be noticed that for compressible lubrication the speed parameter Λ and the load parameter C_L cannot be combined in a manner similar to the Sommerfeld number of incompressible lubrication. This fact is due to the nonlinearity of the governing equation.

It is clear that the amount of information necessary to exhaust all possible interesting geometries and running conditions can assume colossal proportions. Our attitude was to investigate rather thoroughly the geometries which

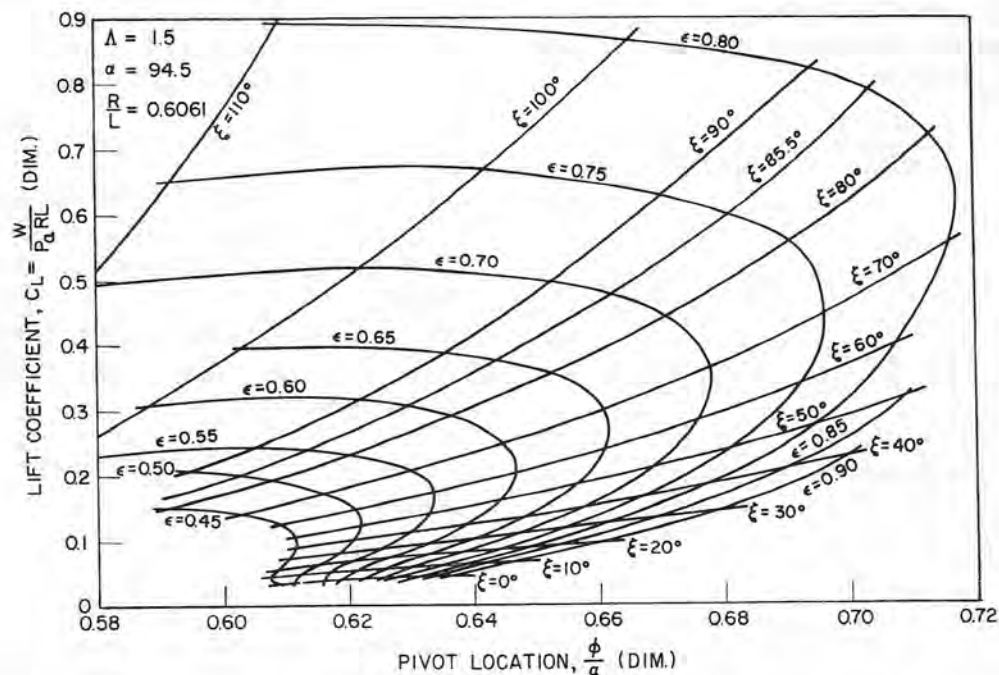


FIG. 3. Theoretical performance of pivoted partial gas journal bearing for $\Lambda = 1.5$

were closely connected with other work at the authors' laboratories and also to make the program available to anyone interested in obtaining more data. Two values of angular extent were investigated: $\alpha = 120^\circ$ and $\alpha = 94.5^\circ$. The first angle closely approximates symmetrical three shoe arrangements. The second was actually used for a practical design where the unidirectionality of the

load made it preferable to space the lower pivots 100° apart rather than at an angle of 120° .

For the $\alpha = 120^\circ$ runs the aspect ratio parameter R/L was given values of $\frac{1}{3}$ and $\frac{1}{2}$. For the $\alpha = 94.5^\circ$ case the values of R/L employed were the ones dictated by the actual parts of the experimental machine under test. These were $R/L = 0.6061$. The actual tabulation of data

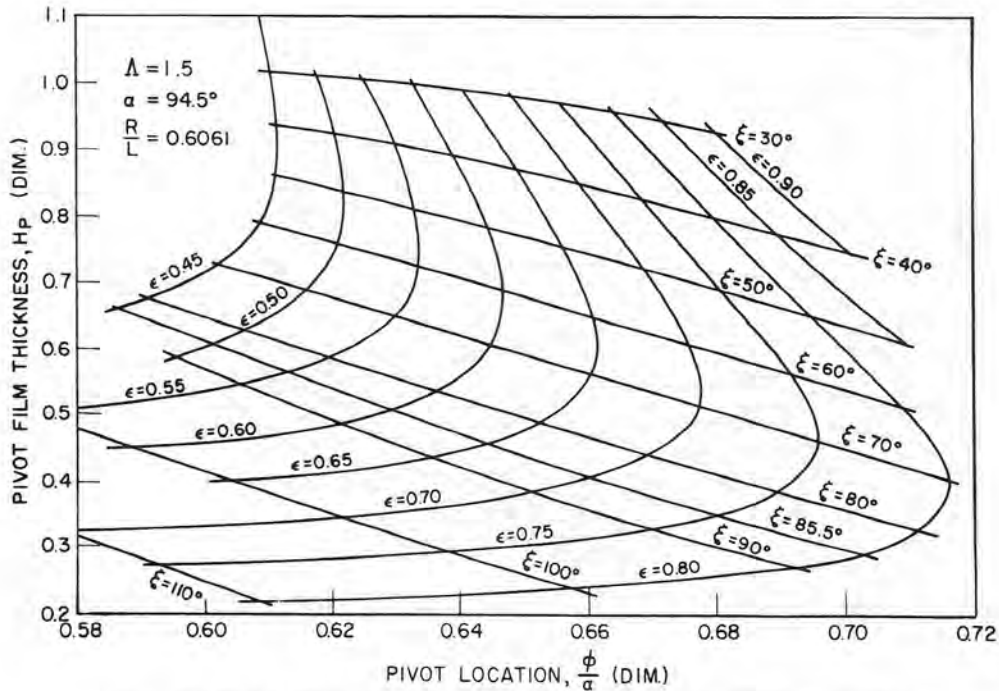


FIG. 4. Theoretical performance of pivoted partial gas journal bearing for $\Lambda = 1.5$

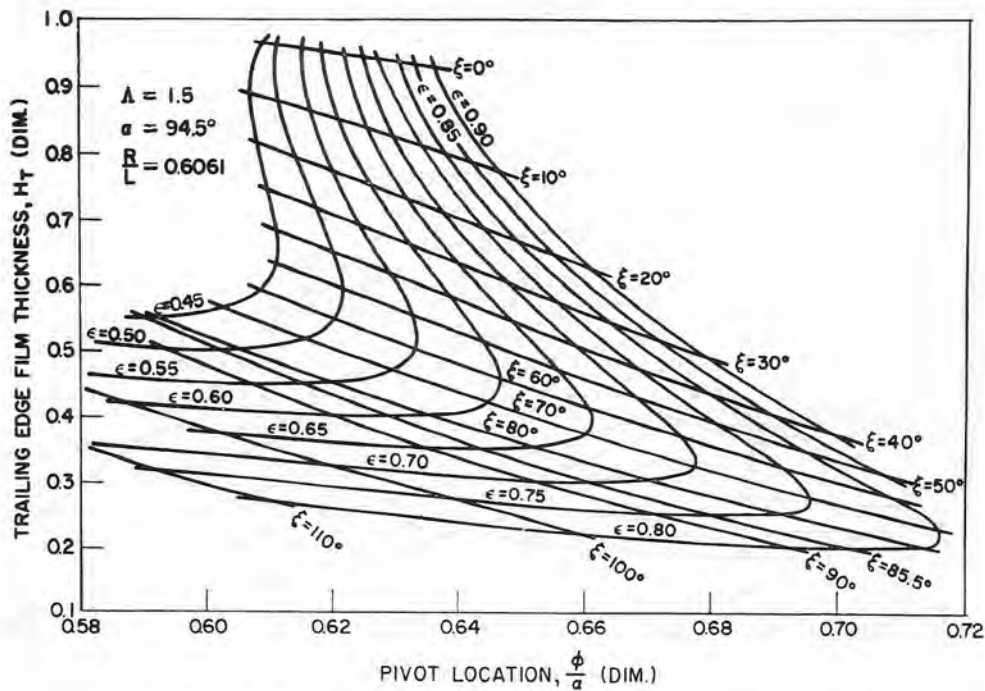


FIG. 5. Theoretical performance of pivoted partial gas journal bearing for $\Lambda = 1.5$

is very lengthy and is not contained herein. However, it is worth mentioning that all computer data plotted so smoothly that no point would fall off the lines presented in the figures. Another important factor in assessing the value of the present solution is that actual checks of theory against experiment were performed with extremely favorable results.

Figures 3-17 contain the above mentioned field maps for values of the bearing parameter Λ of 1.5, 2.5, 3.0, 3.5, and 4.0. These values of Λ are representative of typical operating conditions. The effects of compressibility present in a bearing geometry are not completely represented by the value of Λ . This is due to the fact that Λ is based on the ground clearance "C" between the bearing pad

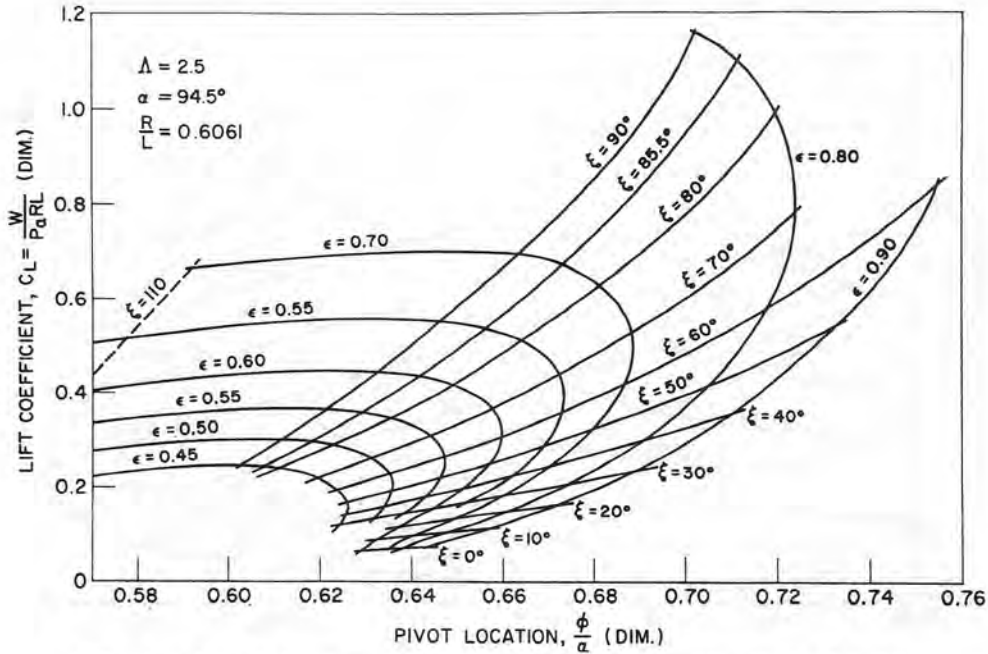


FIG. 6. Theoretical performance of pivoted partial gas journal bearing for $\Lambda = 2.5$

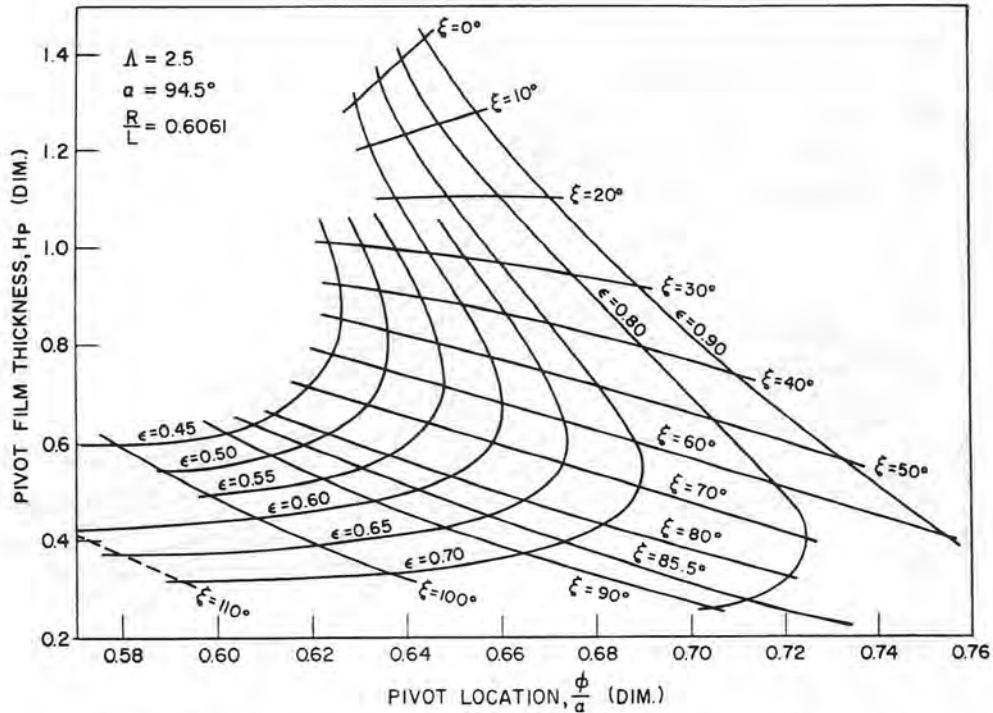


FIG. 7. Theoretical performance of pivoted partial gas journal bearing for $\Lambda = 2.5$

and the shaft. According to the values of ϵ and ξ the value of the actual clearance and particularly the value of the trailing edge clearance can be much lower. For this reason the value of Δ_T (the compressibility parameter based on the trailing edge film thickness) more closely represent the extent of the compressibility effects in the bearing film.

Use of field maps

The characteristics of various bearing arrangements can be predicted by proper use of charts 3-17. In all

the calculations frictional forces will be neglected in comparison to pressure forces. All fixed geometries can be easily analyzed because, for any position of the shaft within the bearing, the exact geometry of each bearing film is known (ϵ and ξ). Then charts 3, 6, 9, 12, and 15 give directly the loads and points of application of the loads in each bearing segment. Vector addition of the loads gives the total load and attitude angle.

In particular, axial groove cylindrical bearings have pads characterized by a common value of ϵ equal to the eccentricity ratio of the shaft within the bearing circle. On a constant ϵ line the pads correspond to values of ξ

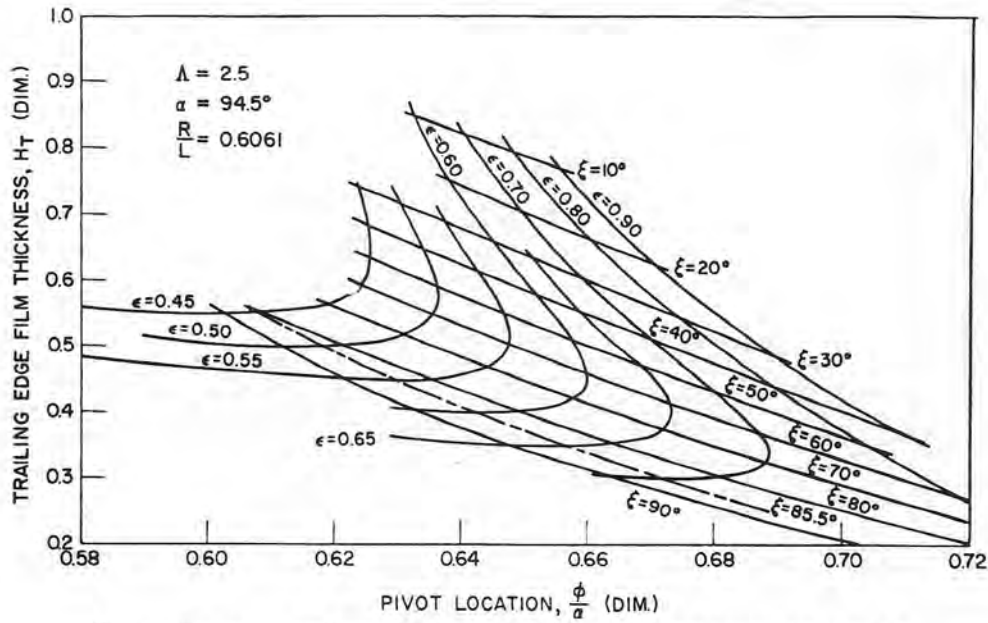


FIG. 8. Theoretical performance of pivoted partial gas journal bearing for $\Lambda = 2.5$

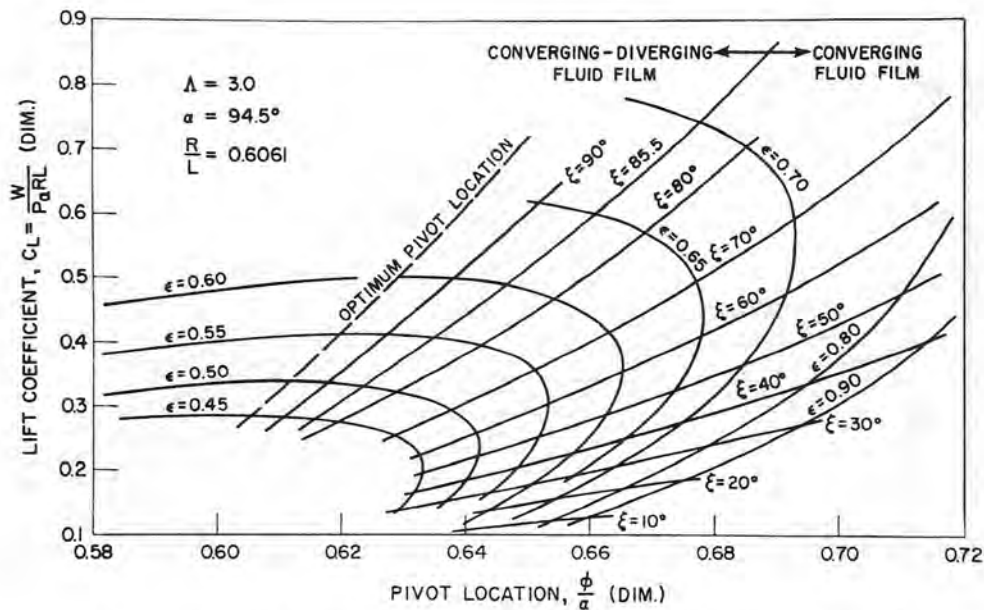


FIG. 9. Theoretical performance of pivoted partial gas journal bearing for $\Lambda = 3.0$

starting from an arbitrary number ξ_0 and spaced at intervals equal to α (angular extent of the pads). Vector addition of the loads will produce a total load and attitude angle corresponding to each selection of ξ_0 :

$$C_L = f(\xi_0)$$

$$\delta = \text{attitude angle} = g(\xi_0)$$

In general, it will be of interest to select only the solution for which $\xi_0 - \delta = \xi_0' = \text{angle between load line}$

and leading edge of first pad (see Fig. 18). The independence of Λ from the shaft position is a great asset in these calculations. Indeed, bearing parameters based on any of the individual pad clearances would require cross-plotting of the data to have Λ on one of the coordinate axes and maps of constant eccentricity. Supplementary nomographs relating Λ to geometry would also be needed.

In the treatment of pivoted-pad bearings the geometry

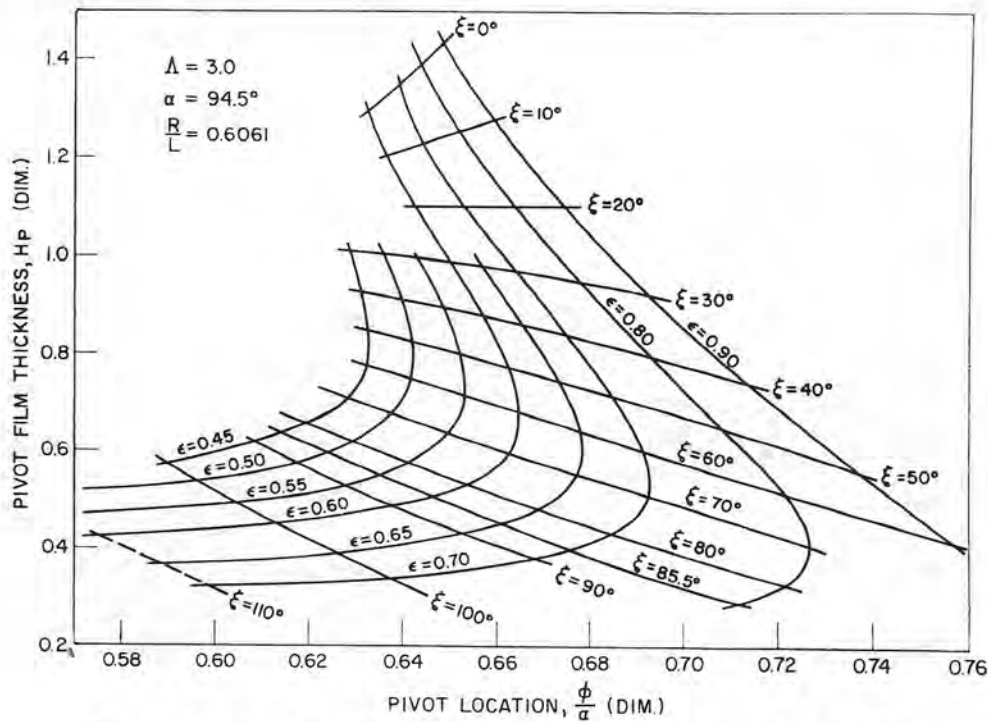


FIG. 10. Theoretical performance of pivoted partial gas journal bearing for $\Lambda = 3.0$

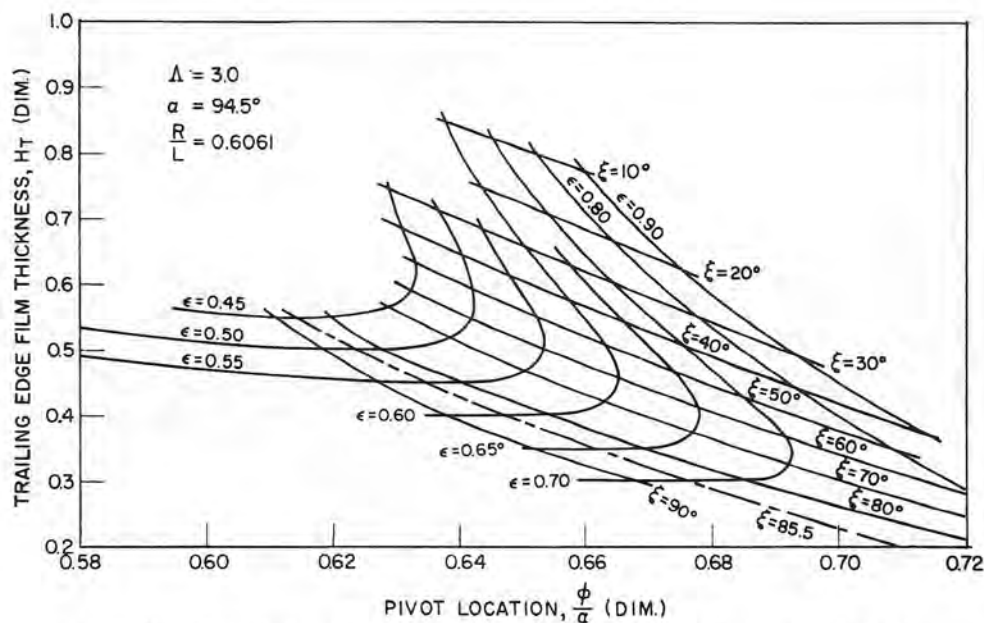


FIG. 11. Theoretical performance of pivoted partial gas journal bearing for $\Lambda = 3.0$

becomes more complicated. Figure 19 shows this type of bearing arrangement for the three shoe case with symmetry about a vertical diameter.

The invariant characteristic of a working pivoted pad is the position of its pivot and—at any journal speed—the value of Λ . This means that all information possibly pertaining to the problem is contained on appropriate vertical lines of Figs. 3–17. Then, for any position of

the shaft within the pivot circle (characterized by the eccentricity ratio ϵ' and the attitude angle δ'), the pivotal clearances H_p are known. One of the graphs of H_p vs. ϕ/α (the one for the appropriate value of Λ) will translate this information into the values of ϵ and ξ for each pad. The graphs of C_L vs. ϕ/α will now be used to obtain the vector loads through each of the pivots. The vectorial addition of the component loads produces

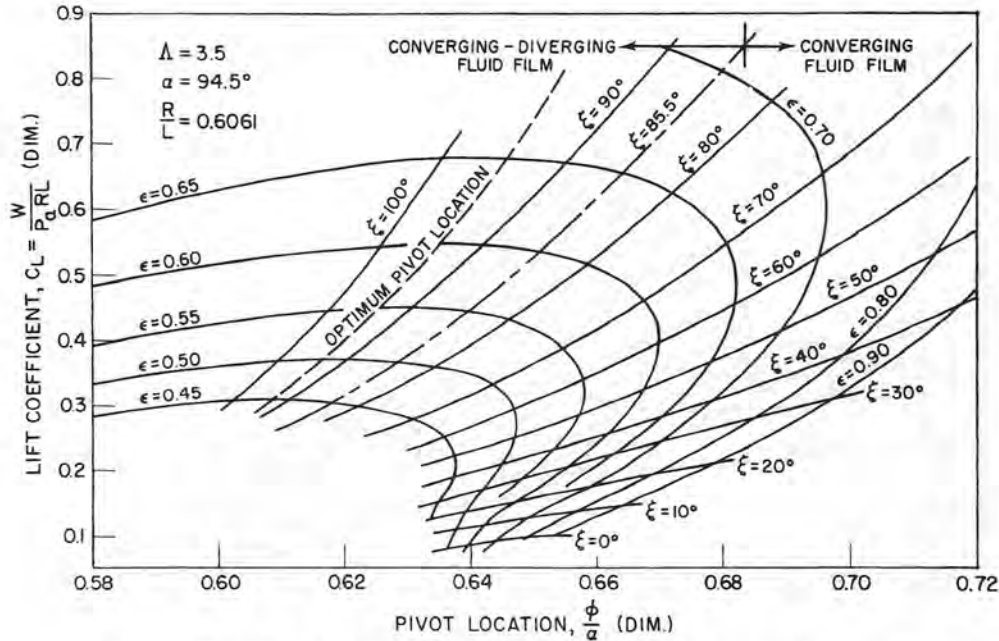


FIG. 12. Theoretical performance of pivoted partial gas journal bearing for $\Lambda = 3.5$

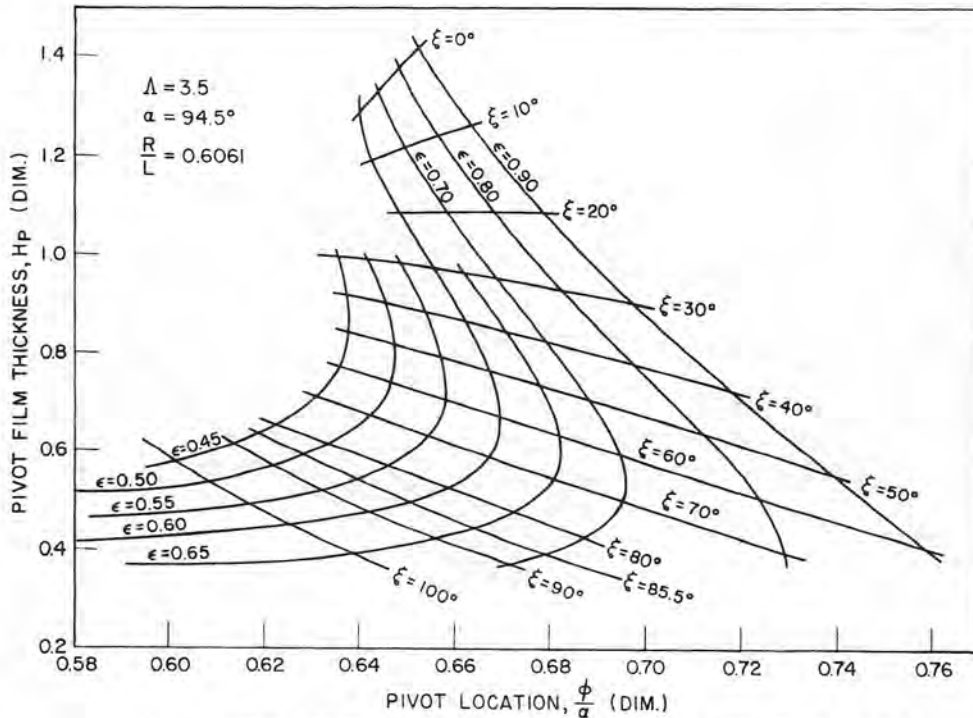


FIG. 13. Theoretical performance of pivoted partial gas journal bearing for $\Lambda = 3.5$

the total load vector. For any eccentricity ratio ϵ' , trial-and-error techniques have to be used in selecting a value of δ' resulting in a total load in the wanted direction.

Considerable simplification is afforded by special geometries such as the one with symmetry about a vertical diameter. In this case the attitude angle is known to be zero and the trial-and-error procedure is no longer necessary. As an example let us consider the problem of evaluating the total C_{LT} vs. ϵ' relation at any particular

value of the bearing speed parameter Λ . For this case (see Fig. 19), $\alpha = 94.5^\circ$ (three equal pads), $R/L = 0.6061$, $\Lambda = 3.5$, and $\beta = 50^\circ$. Then the pivot clearances are given by

$$H_{P_1} = H_{P_2} = (C'/C) [1 + \epsilon' \cos (\Pi - \beta)] \\ = (C'/C) [1 + 0.643 \epsilon']$$

$$H_{P_3} = (C'/C) (1 + \epsilon' \cos C^0) = (C'/C) (1 + \epsilon')$$

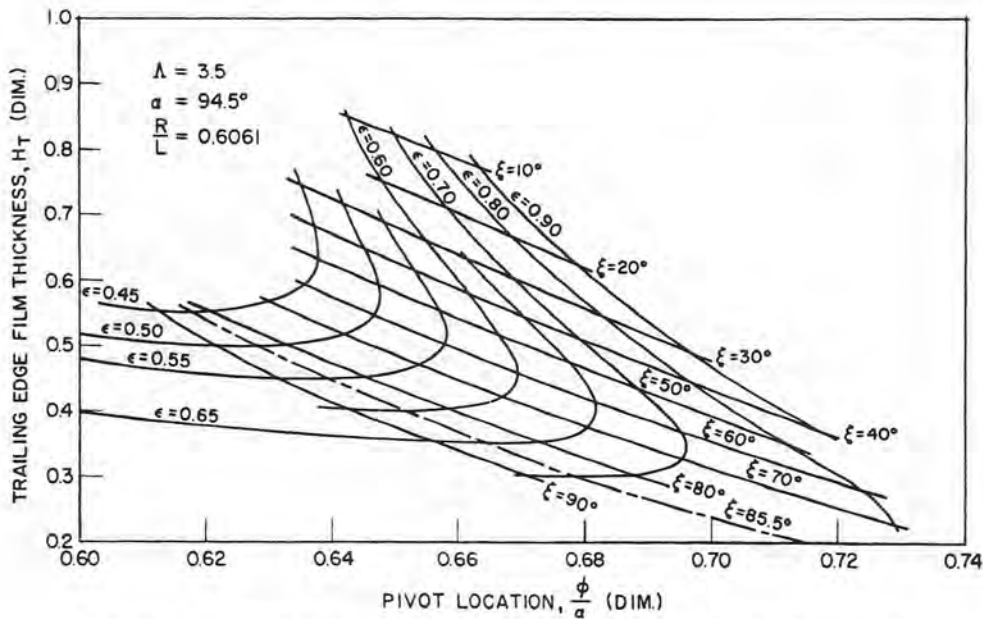


FIG. 14. Theoretical performance of pivoted partial gas journal bearing for $\Lambda = 3.5$

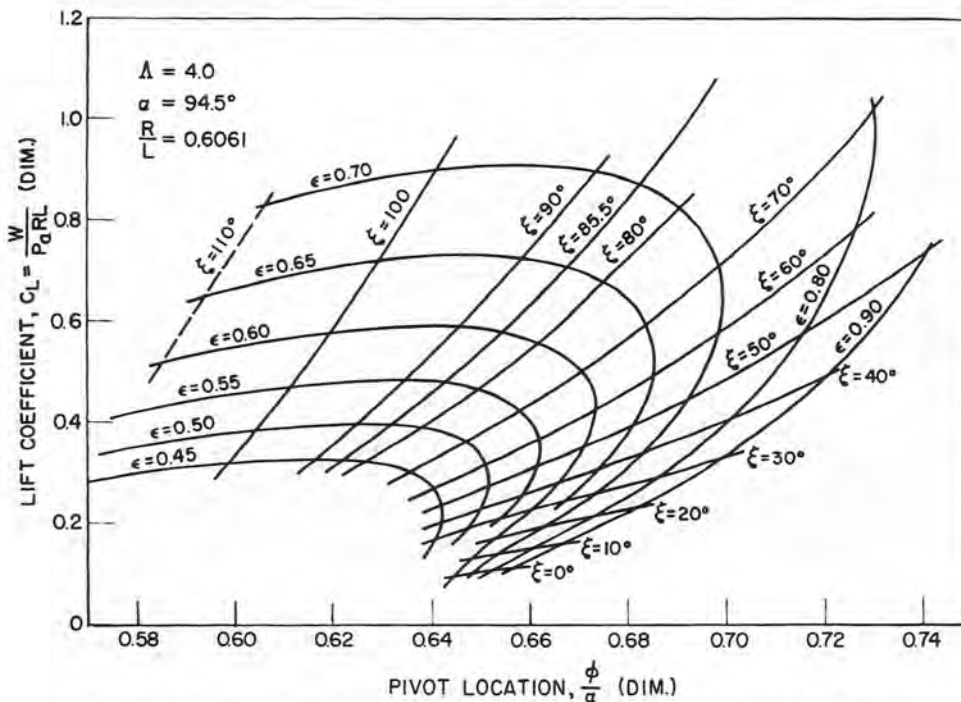


FIG. 15. Theoretical performance of pivoted partial gas journal bearing for $\Lambda = 4.0$

From the values of C_{L1} , C_{L2} , C_{L3} , the total load carrying capacity is obtained as

$$C_{LT} = 2 C_{L1} \cos \beta - C_{L3}$$

or

$$C_{LT} = 1.286 C_{L1} - C_{L3}$$

The values of C_{L1} , C_{L2} , and C_{L3} are obtained by (a) entering Fig. 13 with the proper values of H_P and ϕ/α ,

reading out the corresponding ϵ 's and ξ 's, and (b) entering Fig. 12 with ϕ/α , ϵ , and ξ and reading out C_L . After step (a) the values of ϵ , ξ , and ϕ/α can be used to enter chart 14 and read out H_T . These calculations are shown in Table 1 for values of C'/C equal to 0.6, 0.8, and 1.0; the results are plotted in Fig. 20.

An example of the use of a plot such as Fig. 20 is given by the following problem:

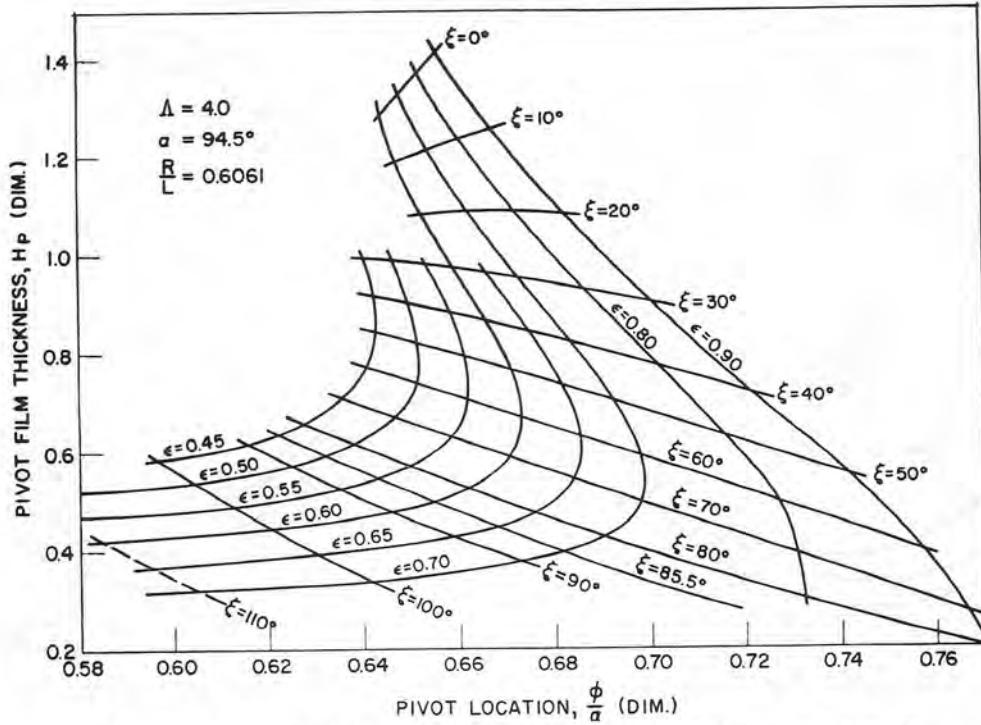


FIG. 16. Theoretical performance of pivoted partial gas journal bearing for $\Lambda = 4.0$

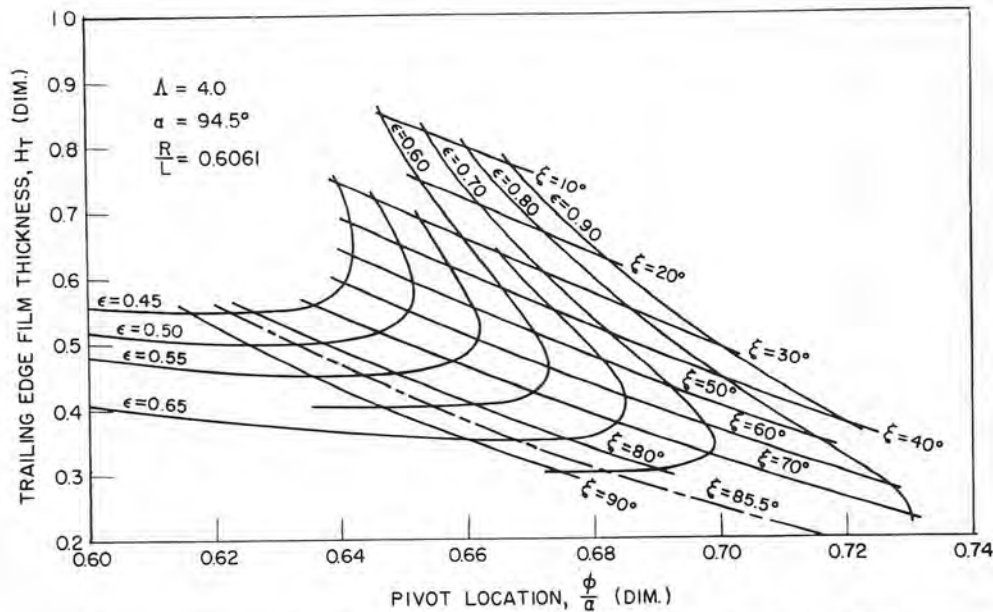


FIG. 17. Theoretical performance of pivoted partial gas journal bearing for $\Lambda = 4.0$

Given: Rotor weight = 80 pounds
 Rotor radius = 2 inches
 Pad axial length = 3.3 inches
 $C = 1.5 \times 10^{-3}$ inches
 Angular velocity = 17,650 rpm

Find: Trailing edge film thickness, running eccentricity, and stiffness corresponding to various values of pivot circle setting.

Procedure: $C_L = \frac{\text{Load}/2}{p_a RL}$

$$\Lambda = \frac{6\mu \omega R^2}{p_a C^2} = \frac{6(2.61 \times 10^{-9})(17650/60) 2\pi(2)^2}{14.7(1.5 \times 10^{-3})^2} = 3.5$$

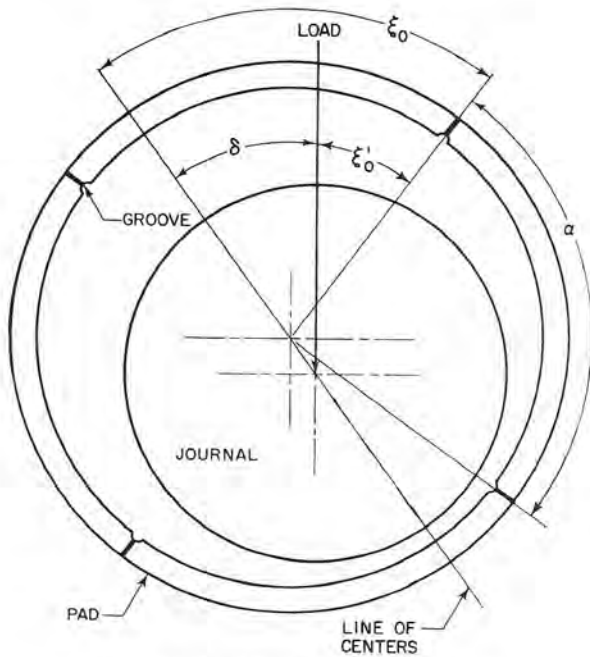


FIG. 18. Axial groove bearing geometry

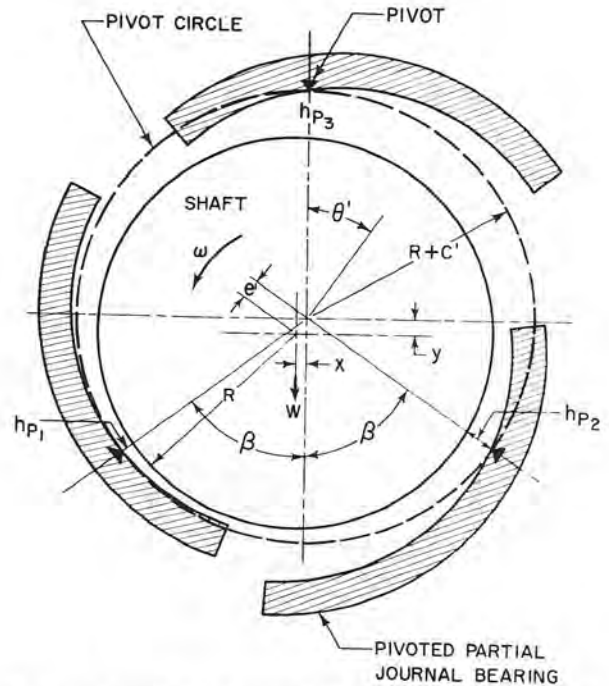


FIG. 19. Pivoted pad journal configuration with three shoes

TABLE 1
 Sample Calculations

	$H_{P_1} = H_{P_2}$	H_{P_3}	ϵ'	ϵ_1	ξ_1	ϵ_3	ξ_3	C_{L_1}	C_{L_3}	C_L	H_{T_1}
$C'/C = 0.6$	0.60	0.60	0	0.595	69.5°	0.595	69°	0.452	0.452	0.1293	0.43
	0.56142	0.66	0.1	0.605	73°	0.585	62°	0.495	0.400	0.2366	0.41
	0.52284	0.72	0.2	0.62	77°	0.59	55°	0.540	0.350	0.3344	0.39
	0.48426	0.78	0.3	0.635	81°	0.60	48°	0.610	0.315	0.4695	0.37
	0.44568	0.84	0.4	0.6503	85°	0.62	41.5°	0.670	0.285	0.5766	0.35
	0.4071	0.90	0.5	0.67	88°	0.65	36°	0.745	0.255	0.7031	0.33
	0.36852	0.96	0.6	0.695	91.5°	0.685	30°	0.845	0.232	0.8547	0.31
$C'/C = 0.80$	0.80	0.80	0	0.605	47°	0.605	47°	0.305	0.305	0.0872	0.53
	0.7486	0.88	0.1	0.595	51.5°	0.635	38°	0.33	0.265	0.1594	0.51
	0.6971	0.96	0.2	0.590	58°	0.68	30°	0.365	0.232	0.2374	0.48
	0.6457	1.04	0.3	0.585	63°	0.74	24°	0.405	0.208	0.3128	0.455
	0.5942	1.12	0.4	0.60	70°	0.81	18.5°	0.460	0.18	0.4116	0.425
	0.5428	1.20	0.5	0.615	75°	0.88	13.5°	0.520	0.16	0.5087	0.400
	0.4914	1.28	0.6	0.635	80.5°	0.93	10°	0.595	0.145	0.6202	0.370
$C'/C = 1.0$	1.00	1.0	0	0.71	27.5°	0.71	27.5°	0.215	0.215	0.0615	0.63
	0.9357	1.10	0.1	0.67	32°	0.795	19.5°	0.240	0.186	0.1226	0.60
	0.8714	1.20	0.2	0.635	39°	0.88	14°	0.266	0.165	0.1771	0.57
	0.8071	1.30	0.3	0.61	46°	0.94	9°	0.300	0.140	0.2458	0.537
	0.7428	1.40	0.4	0.59	52°	—	5°	0.335	0.125	0.3058	0.51
	0.6785	1.50	0.5	0.585	60°	—	2°	0.380	0.110	0.3787	0.47
	0.6142	1.60	0.6	0.591	68°	—	0°	0.44	0.100	0.4658	0.435

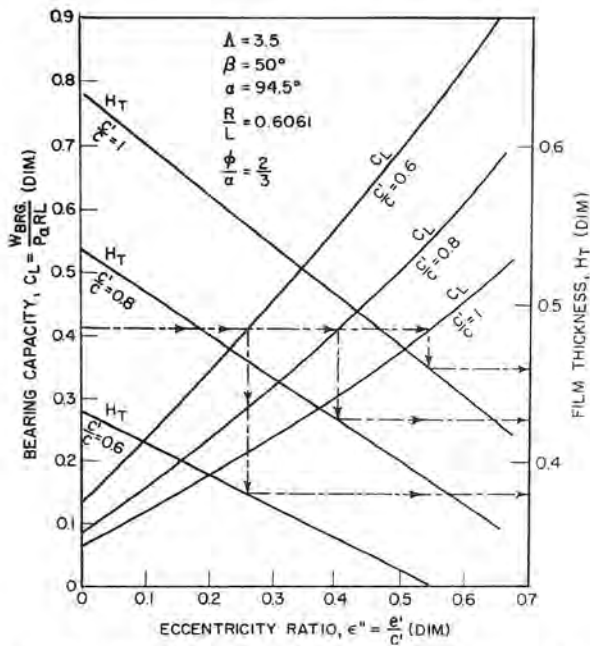


FIG. 20. Sample C_D vs. ϵ' curves for various values of C'/C

Using Fig. 20

C'/C	ϵ'	H_{T1}
0.6	0.26	0.379
0.8	0.40	0.427
1.0	0.54	0.460

$h_{T'} \text{ (in)}$	$\frac{\partial C_L}{\partial \epsilon'}$	$\frac{\partial W}{\partial e} \text{ (lb/in)}$ per bearing
0.569×10^{-3}	1.14	1.23×10^5
0.640×10^{-3}	0.91	0.736×10^5
0.690×10^{-3}	0.80	0.517×10^5

where the stiffness (per bearing) is

$$\frac{\partial W}{\partial e} = \frac{\partial C_L}{\partial \epsilon'} \left[\frac{p_a R L}{C(C'/C)} \right] = \frac{\partial C_L}{\partial \epsilon'} \left(\frac{64.6 \times 10^3}{C'/C} \right)$$

From the results it can be seen that the preload parameter C'/C has a marked effect on the operation of pivoted-pad gas bearings. Particularly noticeable is the effect of C'/C on the stiffness which can be interpreted as a valuable tool for a posteriori adjustment of the rotor critical speed. Since it is well known that the self-excited whirl threshold speed is some multiple of the rotor critical speed (approximately twice for small attitude angles), the whirl instability region can be modified within limits by proper setting of the pivot circle clearance.

ACKNOWLEDGMENTS

This research was supported by the Department of Defense, AEC, NASA, under contract No. Nonr-2342(00) FBM (c) Task NR 062-316 administered by the Office of Naval Research. The authors are indebted to S. W. Doroff, ONR Project Supervisor; J. C. Reid, Jr., Code 644, Bureau of Ships; and the staff of the David Taylor Model Basin Applied Mathematics Section.

REFERENCES

1. SNELL, L. N., "Pivoted-Pad Journal Bearings Lubricated by Gas," IGR-R/CA-285, United Kingdom Atomic Energy Authority, Industrial Group, 1958.
2. GROSS, W. A., "Numerical Analysis of Gas-Lubricating Films," Proceedings, First International Symposium on Gas-Lubricated Bearings, Office of Naval Research, Dept. of the Navy, ACR-49, October 1959, U.S. Government Printing Office, Washington 25, D. C.
3. FORSYTHE, G. E., and WASOW, W. R., "Numerical Methods for the Solution of Partial Differential Equations." Wiley, New York, 1960.
4. GUNTER, E. J., CASTELLI, V., and FULLER, D. D., "Theoretical and Experimental Investigation of Gas-Lubricated, Pivoted-Pad Journal Bearing," *ASLE Trans.* 6(4), October 1963.

DISCUSSION

L. LICHT (IBM, Thomas Watson Research Center, P.O. Box 218, Yorktown Heights, New York):

The contributions, the ASME paper 63-Lub-5, by Wernick and Pan, and the ASLE paper 63-LC-6, by Castelli, Stevenson and Gunther, presented during the Gas-Bearing Session of this ASLE-ASME Lubrication Conference, included complementary methods of approach to the problem of partial-arc and pivoted gas-bearings.

The method of Wernick and Pan is limited to small values of the bearing number, Λ , and is essentially a perturbation solution. Approximating expressions are given for radial and tangential film-force components in series form and the numerical work involved appears to be not inconsiderable. The question, therefore, arises, whether it is more profitable to attempt "exact," finite-

difference solutions by going directly to the computer (Castelli, Stevenson, Gunther), or whether there is a greater advantage in obtaining approximate results by means of the Galerkin method (Wernick, Pan) and then delegating to the computer a presumably simpler to program and less time-consuming amount of numerical work. Undoubtedly, the authors of both papers would like to comment on relative advantages and/or disadvantages of each method.

EDITOR'S NOTE:

Authors are furnished a copy of each discussion and invited to submit a closure. Since no closure was submitted for the above article, it may be assumed that the authors either concurred with the discussor or did not feel that a reply was necessary.